A Crack Layer Approach to Fatigue Crack Propagation in High Density Polyethylene

M. L. KASAKEVICH* and A. MOET, *Department of Macromolecular Science, Case Western Reserve University, Cleveland, Ohio 44106,* and A. CHUDNOVSKY, *Department of Civil Engineering, Mechanics and Materials, University of Illinois-Chicago, Chicago, Illinois 60680*

Synopsis

Fatigue crack propagation (FCP) in high density polyethylene (HDPE) is observed to occur with an accompanying layer of damage ahead of the crack tip. The crack layer theory, which accounts for the presence of both the damage and the main crack, is applied to the problem. It is observed that the kinetic behavior of HDPE under fatigue consists of three regions: initial acceleration, constant crack speed ("deceleration"), and reacceleration to failure. Within the first two regions, crack propagation appears "brittle," while in the third region "ductile" behavior is manifested. Ultimate failure occurs via massive yielding of the unbroken ligament. Two damage mechanisms are found to be responsible for HDPE failure: formation of fibrillated voids and yielding. Both mechanisms are present throughout the entire lifetime of the crack, but the former dominates the "brittle" crack propagation region, while the latter is more prominent in the "ductile." Throughout the analysis the resistance moment R_t is approximated as the total volume of transformed material associated with crack advance. Crack layer analysis produces a satisfactory fit of the experimental data and yields a specific enthalpy of damage, γ^*, value in the 1–2 cal/g range.

INTRODUCTION

It is well known that medium density polyethylene (MDPE) is much more resistant to crack propagation than high density polyethylene (HDPE) despite the similarity in their moduli and yield stress values.[1] Furthermore, it has been shown that some varieties of MDPE are much less resistant to crack growth than others with virtually identical moduli and yield stresses.[2,3] It is clear, therefore, that gross mechanical parameters (E and σ_y) do not provide an adequate basis for the description and prediction of a material's ability to resist crack propagation. On the other hand, the resistance to crack propagation is an extremely important criterion for lifetime prediction in load bearing engineering components and there exists a need for the establishment of an analytical framework within which a reasonable assessment of lifetime can be achieved.

Since macroscopic mechanical parameters fail to predict material resistance to crack propagation, this behavior must be determined by the morphological and chemical microstructure of the material. The manner in which a given material reacts to stress and distributes it in the vicinity of the crack tip will determine its resistance to crack propagation. For polymers this reaction occurs on the morphological level, but morphology itself is determined to a

*Present address: Shell Development Company, P.O. Box 1380, Houston,TX 77251.

Journal of Applied Polymer Science, Vol. 39, 395–413 (1990)
 CCC 0021-8995/90/020395-19$04.00

large extent by molecular structure and both must be considered in any model striving to achieve physical understanding of crack propagation resistance.

Traditionally, polyethylene crack propagation behavior has been studied through application of linear elastic fracture mechanics (LEFM).[4-6] This approach treats the crack as an ideal cut in an elastic body and proposes the stress intensity factor K or, alternatively, the elastic energy release rate $G = K^2/E$ as the driving force for crack propagation. Although fruitful in some respects, this approach does not address the question of material resistance to crack propagation, since the ideal cut approximation does not allow for the presence of morphological and molecular variables.

Other ubiquitous approaches to fracture behavior analysis, include the Paris equation.[7,8] It too, however, fails to provide physical insight into the crack propagation phenomenon. The Paris equation relies on LEFM parameters and is, therefore, also unable to reflect variations in material morphology and chemical structure. The phenomenological coefficients obtained in the Paris analysis have no known physical meaning and reveal nothing about the nature of the failure process.

The crack layer theory[9,10] provides the desired link between crack propagation resistance of a material and its microstructure. It considers the crack and the surrounding zone of damage as a single thermodynamic entity—the "crack layer" (CL). The resulting equation of rectilinear crack propagation is

$$dl/dt = \dot{D}/(\gamma^* R_t - A_1)$$

where dl/dt is the crack speed, $\dot{D}$ the rate of energy dissipation on damage creation within the active zone, and γ^* the specific enthalpy of damage. R_t is the total resistance moment to crack propagation and reflects the magnitude of damage associated with crack advance. A_1 is the total potential energy release rate.

Thus, although two chemically different polymers such as poly(methyl methacrylate) (PMMA) and polystyrene (PS) can both exhibit damage in the form of crazes, they are distinguished within this treatment on the basis of the $\gamma^* R_t$ term. The energetic "cost" of craze creation will be different for each polymer and this difference will be reflected in the specific enthalpy of damage. All of the individual crack layer parameters will be discussed in greater detail in later sections, but at this stage the equation serves as an illustration of how material microstructure can be utilized (through the $\gamma^* R_t$ term) in conjunction with the total energy release rate A_1 to rationalize crack propagation behavior of a given material. It is this specificity of the theory to structural variations among different materials which makes it particularly useful.

In this paper the crack layer theory will be applied to fatigue crack propagation in HDPE.

EXPERIMENTAL

The polyethylene used was a high density (0.964 g/mL) homopolymer with a melt flow index of 0.75, M_n = 19,600 and M_w = 130,000. The material was supplied in bead form by Phillips Petroleum (Marlex 6006).

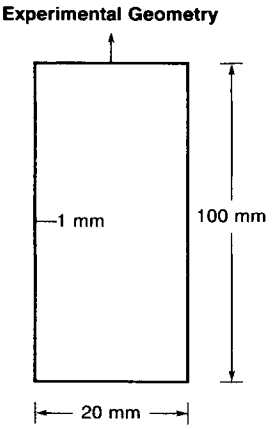

Fig. 1. Experimental geometry.

HDPE sheets of 0.6–0.7 mm thickness were compression-molded at 190°C and 20,000 psi and then allowed to cool slowly to room temperature in the press. Strips of 140 × 20 mm dimensions were cut from the sheets with a razor blade. These samples were then notched on the edge with a fresh razor blade to a 1.0 mm depth and crack propagation tests were performed under tension–tension fatigue conditions using an MTS machine (see Fig. 1 for specimen geometry). The loading waveform applied was sinusoidal with a frequency of 0.5 Hz. Samples were tested under mean stresses of 7.94 and 3.75 MPa with a load ratio of 0.5 in each case.

The crack tip and the accompanying damage were observed with a traveling optical microscope and recorded on video tape. Subsequent crack length and damage zone measurements were made from these recordings. Load–displacement curves from each sample were recorded throughout the duration of the experiment.

Fracture surfaces were examined with a stereoscope/image analyzer system. Some samples were gold-sputtered and examined in a Jeol JSM 35CF scanning electron microscope under a 15 kV accelerating potential.

Young's modulus and yield stress data were obtained on an Instron universal testing machine for standard specimens. The values were found to be 1100 and 30 MPa, respectively.

RESULTS

Fracture Propagation Kinetics

Figure 2 depicts the propagating fatigue crack and its accompanying damage layer in HDPE at three different crack lengths. In the initial stages of stable crack growth, at $l = 1.3$ mm [Fig. 2(a)] the crack is characterized by a relatively small crack opening displacement, a sharp crack tip, and a rather small, pointed zone of preceding damage. This type of appearance is traditionally associated with a brittle crack under small scale yielding conditions and is treated on the basis of LEFM. By the time the crack reaches a crack length of 5.0 mm [Fig. 2(b)] the crack opening displacement is much greater, the crack

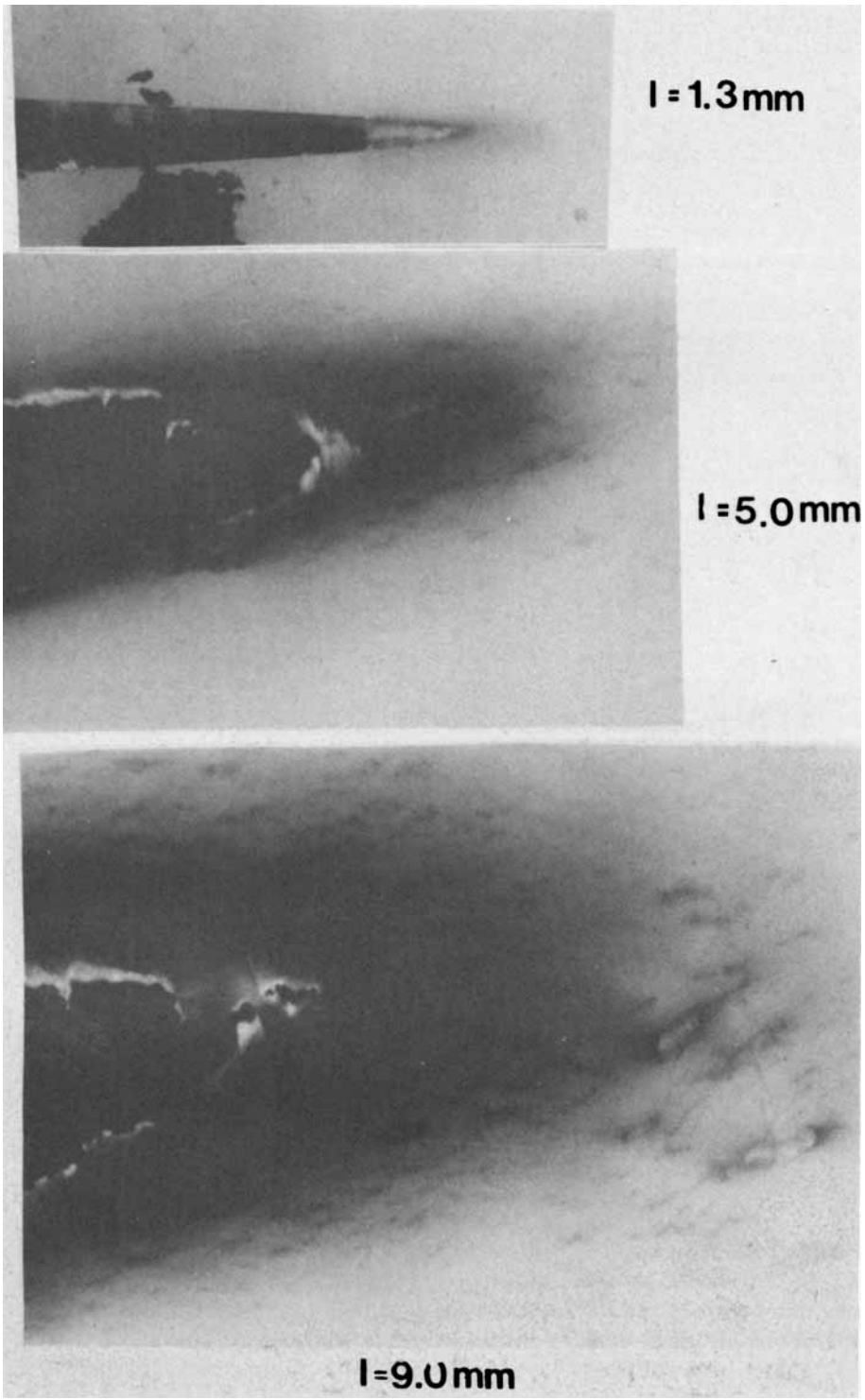

Fig. 2. Optical micrographs of crack tip and damage zone in HDPE fatigue. Magnification is 43 × .

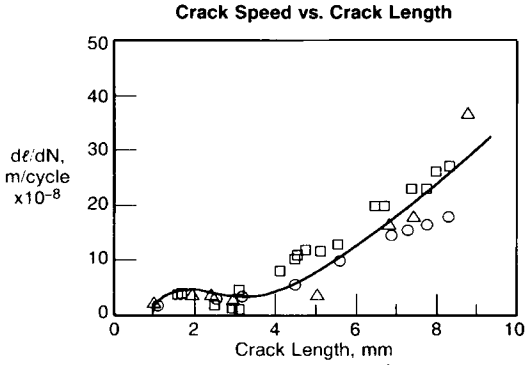

Fig. 3. Crack speed vs. crack length for three identical HDPE fatigue specimens. Mean stress is 7.94 MPa.

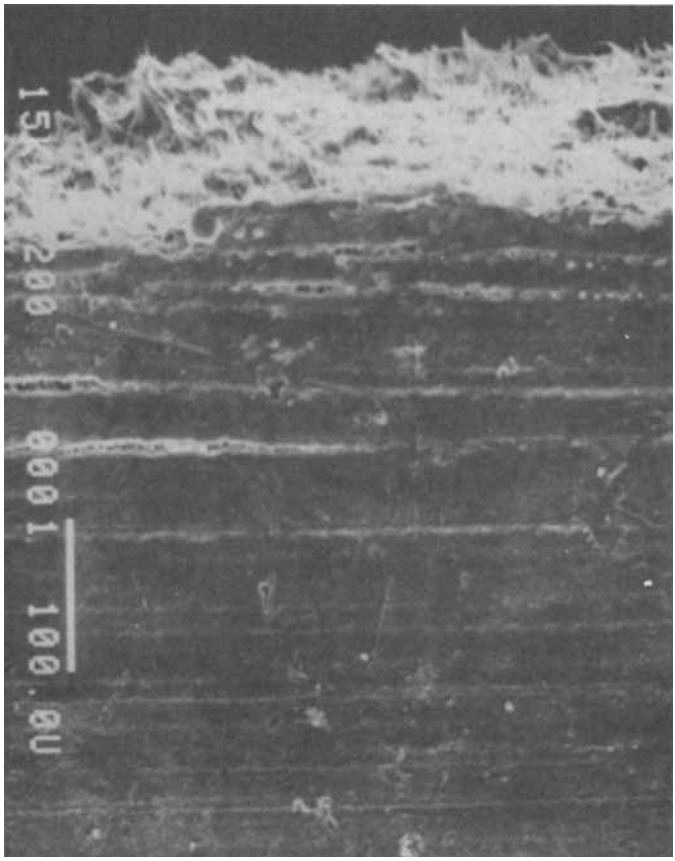

(a)

Fig. 4. 200 × SEM micrographs of the damage zone at l = 4.0 (a), 7.0 (b), and 9.0 (c) mm.

tip is no longer sharp or well defined, and the zone of damage ahead of the crack has expanded significantly and relinquished its pointed nature in favor of a more elliptical shape. At this point the crack is already no longer part of the LEFM domain. In the final stages of stable crack propagation, at $l = 9.0$ mm [Fig. 2(c)], the crack opening displacement is very large, the crack tip completely blunted, and the associated zone of damage quite expansive and more rounded in appearance. All of these attributes are characteristic of a predominantly ductile failure process.

The crack propagation rates of three identical HDPE samples fatigued under a mean stress of 7.94 MPa are plotted as a function of crack length in Figure 3. Other than the initial acceleration region around $l = 1.0$ mm two regions are readily discernible in the kinetic plots. The "deceleration" or constant crack speed region from $l = 1.5$ mm to $l = 4$ mm is virtually identical among the four samples. It is within this region that the crack displays the "brittle" attributes of sharp crack tip and small damage zone. The kinetic region from $l = 4.5$ mm to $l = 9.0$ mm consists of accelerating crack growth and includes the remainder of the stable crack lifetime. Here the samples exhibit more individual behavior, lacking the high degree of reproducibility observed earlier. This region is characterized by the rapidly growing

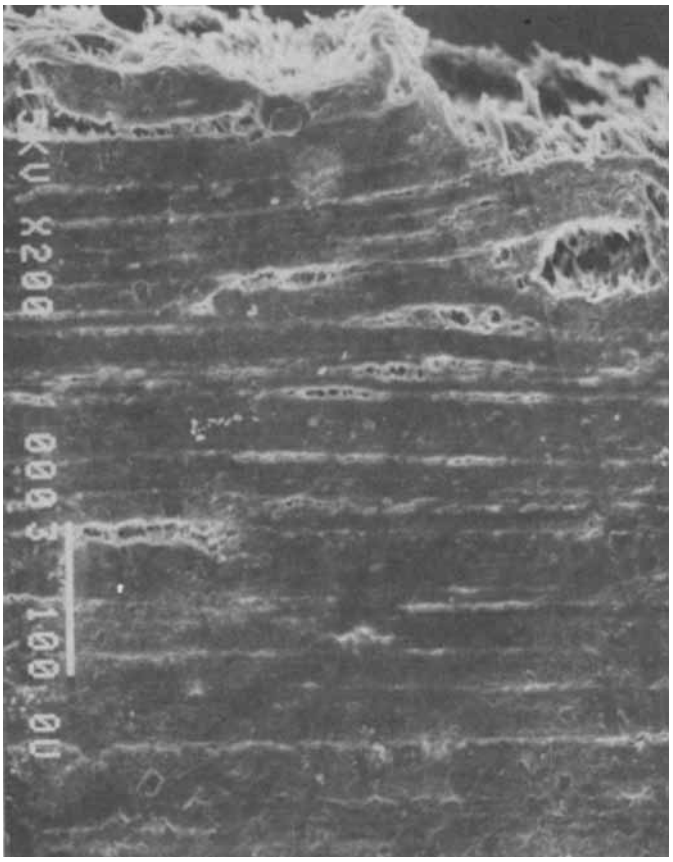

(b)

Fig. 4. (*Continued from the previous page.*)

crack opening displacement, blunted crack tip, and the large, increasingly more rounded zone of damage seen in Figures 2(a) and 2(b). Beyond a crack length of approximately 9 mm the crack accelerates very rapidly and ultimate failure occurs via massive yielding of the unbroken ligament.

It should be mentioned that this type of kinetic behavior is not at all unprecedented for both high density[11,12] and low density[13-15] polyethylenes.

Micromechanisms

To this point the damage preceding the crack tip has been treated in aggregate fashion as a zone. With the help of optical microscopy (OM) and scanning electron microscopy (SEM) the contents of the damage zone can be examined.

Even with the somewhat modest magnification level of Figure 2, one can easily distinguish the presence of large fibrillated craze like entities within the dark damage zone. With the higher magnifications afforded by SEM it becomes apparent that the damage consists of such fibrillated "pores" on a much smaller scale. These grow and coalesce to form the very large voids seen in the optical micrographs of Figure 2. In Figure 4 the SEM micrographs of

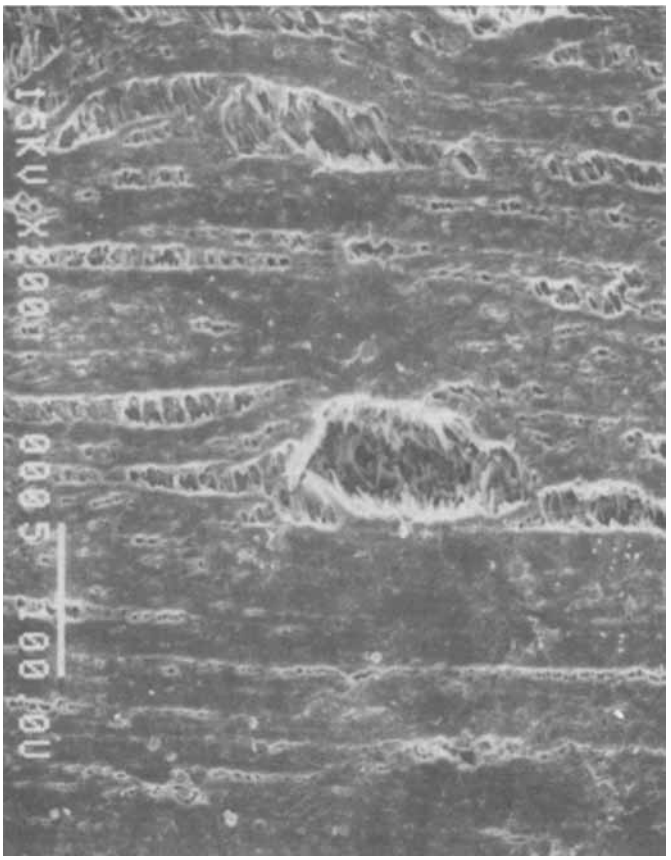

(c)

Fig. 4. (*Continued from the previous page.*)

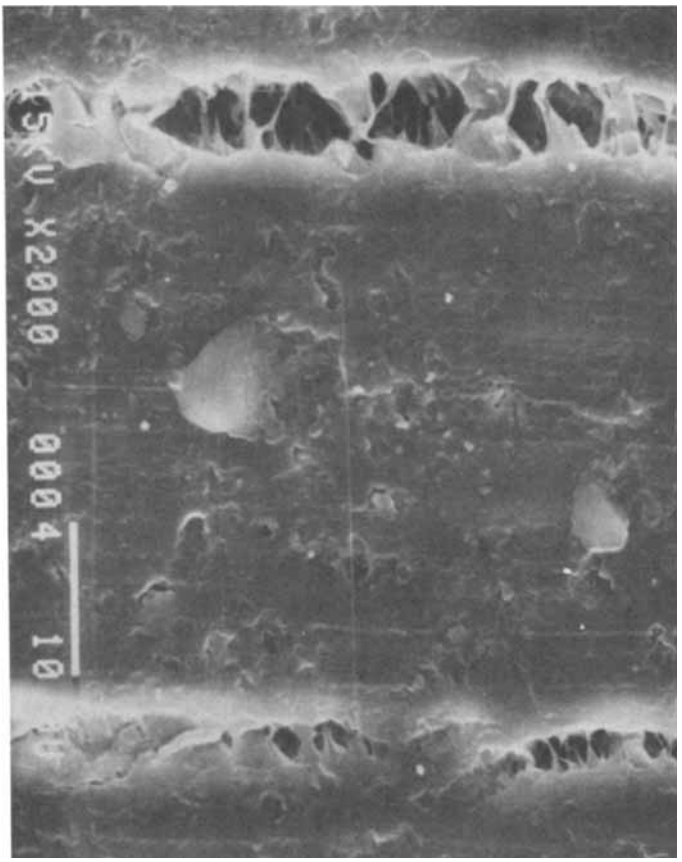

Fig. 5. 2000 × SEM micrograph of an individual fibrillated void.

damaged regions at three different crack lengths suggest that the nature of damage zone composition does not change with crack length. The density of the pores, however, does appear to increase with crack extension. The individual pores are shown in greater detail in Figure 5.

Fibrillated pore formation is only one of the damage mechanisms uncovered in this study. Examination of the fracture surface revealed pronounced yielding which increased significantly with crack growth. The "thinning" profiles for the fatigue samples are shown in Figure 6. It is quite obvious that yielding is present throughout the lifetime of the crack, but it becomes much more rapid past a crack length of approximately 4.5 mm. The reader is reminded that this corresponds well with the changes in crack tip geometry and damage zone size and shape (i.e., the onset of the third kinetic region).

It appears, therefore, that there are two damage mechanisms involved in HDPE fatigue crack growth. Although both are present at all stages of crack propagation, the fibrillated pore mechanism seems to be more prominent in the "brittle" kinetic regions, whereas the yielding mechanism becomes dominant in the "ductile" crack acceleration region.

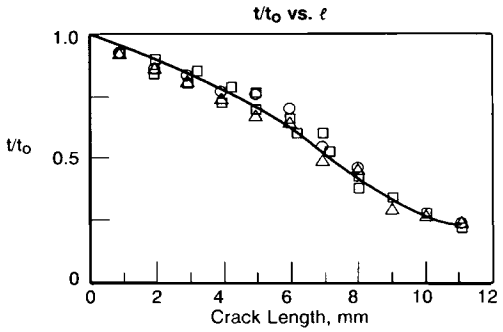

Fig. 6. Thinning profile of HDPE fatigue specimens (t is fracture surface thickness at 1 and t_0 is original thickness). Mean stress is 7.94 MPa.

DISCUSSION

The Crack Layer Formalism and Damage Zone Evolution

As shown in Figure 2 the fatigue crack in HDPE is surrounded by a layer of transformed (damaged) material. The crack layer theory[9,10] considers the crack and its surrounding damage as a single entity—the "crack layer" (CL). The portion of the layer ahead of the crack tip where damage production is nonzero is called the "active zone." CL propagation can be resolved into elementary movements of the active zone such as translation, rotation, isotropic expansion, and distortion (shape changes). This evolution of the active zone for a representative HDPE fatigue sample is shown in Figure 7. Elementary movements of the active zone can be quantified through the active zone deformation tensor shown below:

$$d = \begin{pmatrix} \ln(l_a/l_{a0}) & 0 & 0 \\ 0 & \ln(w/w_0) & 0 \\ 0 & 0 & \ln(t/t_0) \end{pmatrix}$$

where l_a = active zone length (distance from crack tip to active zone tip), w = active zone width (measured across the crack tip), and t = fracture surface thickness. The subscript 0 denotes the values of these parameters at initiation. The coordinate system employed is Cartesian with the crack tip

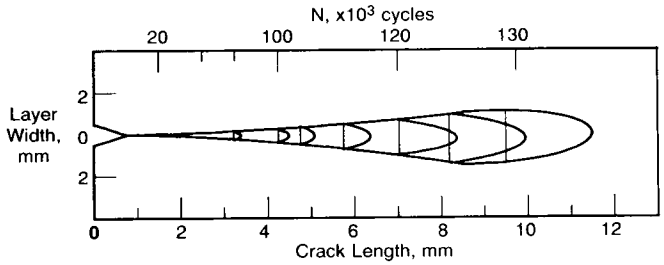

Fig. 7. Schematic of damage zone evolution.

taken as the origin and the l_a axis tangent to crack trajectory. Active zone length and width are available from Figure 7 and fracture surface thickness may be taken at the appropriate crack length from Figure 6.

Isotropic expansion of the active zone can be expressed as

$$e = 3I_1$$

where I_1 is the first invariant of the spherical part of the deformation tensor above.[16] Explicitly this is given by

$$e = \ln(lwt/l_{a0}w_0t_0)$$

Active zone shape changes are expressed quantitatively through the distortion parameter I_d defined as

$$I_d = J_2'$$

where J_2' is the second invariant of the deviatoric part of the deformation tensor.[16] Explicitly it is given by

$$I_d = 1/6\left([\ln(w_0l_a/wl_{a0})]^2 + [\ln(t_0w/w_0t)]^2 + [\ln(l_{a0}t/t_0l_a)]^2\right)^{0.5}$$

Expansion and distortion parameters representing quantitatively these elementary zone movements are plotted as a function of crack length in Figures 8 and 9.

In the crack layer theory elementary movements are presented as fluxes corresponding to reciprocal thermodynamic driving forces. Within the framework of irreversible thermodynamics the product of the driving force with the corresponding flux gives the total entropy production of the process under consideration. In this case, total entropy production is expressed as[17]

$$T\dot{S}_i = X^l dl/dt + X^e de/dt + X^d : dI_d/dt$$

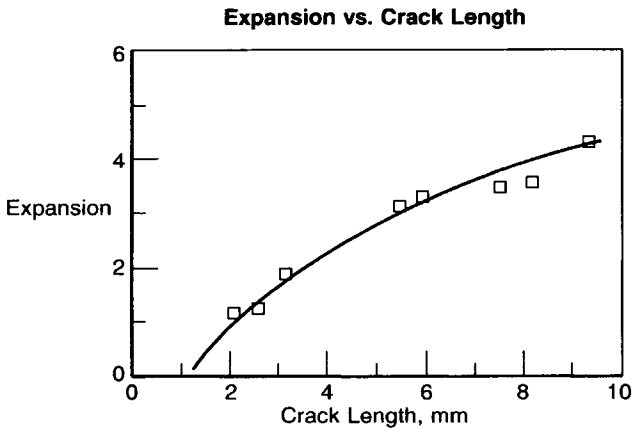

Fig. 8. Active zone expansion plotted as a function of crack length. Mean stress is 7.94 MPa.

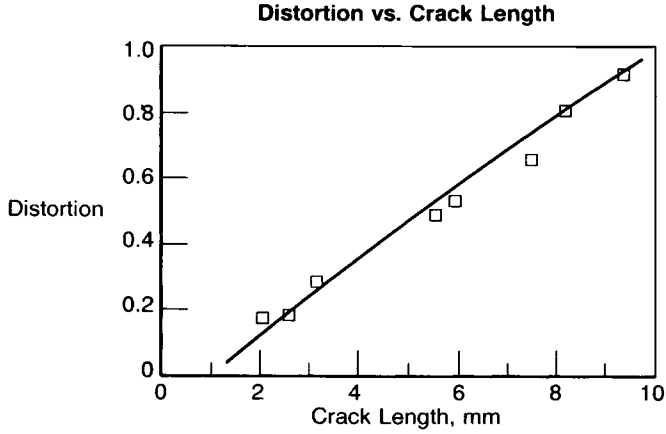

Fig. 9. Active zone distortion plotted as a function of crack length. Mean stress is 7.94 MPa.

where dl/dt is the rate of CL translation, and de/dt and dI_d/dt are the rates of CL expansion and distortion, respectively. X^l, X^e, and X^d are the reciprocal thermodynamic driving forces.

The equation may be resolved further by recognizing that

$$de/dt = \delta_l e\, dl/dt + \delta_t e$$

$$dI_d/dt = \delta_l I_d\, dl/dt + \delta_t I_d$$

Symbols of type δ_z denote partial differentiation with respect to variable z. The partials of expansion and distortion with respect to time represent the dissipative fluxes within the active zone. The product of these with the reciprocal forces yields the rate of energy dissipation on damage creation within the active zone:

$$\dot{D} = X^l \delta_t e + X^d : \delta_t I_d$$

The translational driving force has been identified as[17]

$$X^1 = 1/T(J_1 + M\delta_l e + N : \delta_l I_d) - \gamma^* R_t$$

where J_1, M, and N are the well-known energy release rate integrals of fracture mechanics, γ^* is the specific enthalpy of damage, R_t is the translation resistance moment, and T is the absolute temperature. Physically, R_t may be identified with the amount of material transformed in CL propagation.

Substituting the expressions for $\dot{D}$ and X^l into the equation of total entropy production and applying the principle of minimal entropy production ($\dot{S}_i = 0$)[9] yields

$$dl/dt = \dot{D}/(\gamma^* R_t - A_1)$$

where A_1 is the total potential energy release rate defined as[18]

$$A_1 = J_1 + M\delta_l e + N : \delta_l I_d$$

A_1 differs from the commonly used J_1 in that it accounts for expansion and distortion of the CL. Since both of these effects are clearly present, as shown in Figures 8 and 9, A_1 and not J_1 should be used.

The equation above is the law of CL propagation. The remainder of this paper will be devoted to the evaluation of CL parameters from experimentally accessible quantities.

Evaluation of the Energy Release Rate

The energy release rate A_1 was determined using the conventional method of Landes and Begley.[19] The procedure requires calculation of the area between the loading portions of the load–displacement curves obtained at different crack lengths. Some crack advance may occur during the loading part of the fatigue cycle; hence the unloading curves were used for A_1 evaluation in this study. The actual energy release rate was computed as

$$A_1 = -1/t_0[dP/(l_2 - l_1)]$$

where t_0 is the original sample thickness and dP is the area between unloading curves at crack lengths l_2 and l_1. Physically, dP represents the potential energy change of the specimen associated with the crack advance. It is important to point out here that, although this evaluation method was developed J_1, it, in fact, measures A_1, since some portion of dP is due to active zone movements.

The result of the calculation is plotted as a function of crack length in Figure 10. Also plotted is the elastic energy release rate $G_1 = K^2/E$. As expected, the two curves nearly coincide at shorter crack lengths and are fairly close throughout the "brittle" regime. They diverge quite significantly, however, within the "ductile" crack propagation regime. Neither the existence nor the relative direction of the discrepancy between the two curves is surprising. By no means can one expect G_1, a linear elastic parameter, to be applicable to the type of crack–damage system shown in Figures 2(b) and (c).

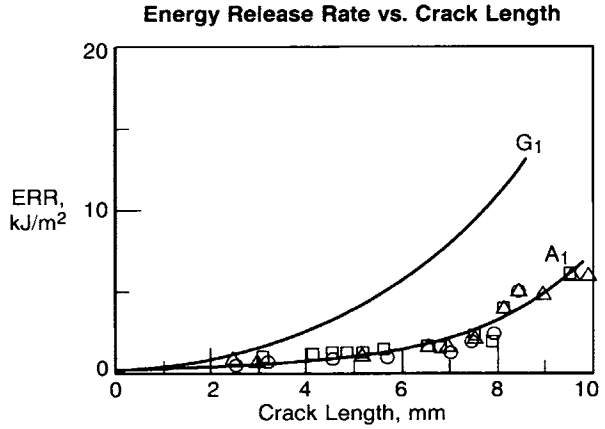

Fig. 10. Total potential energy release rate plotted vs. crack length for three HDPE fatigue specimens. Elastic energy release rate is also plotted. Mean stress = 7.94 MPa.

All types of damage are thought to shield the crack tip from the applied stress, thus reducing the effective stress felt by the material in the vicinity of the crack.[20] Due to this shielding the actual energy release rate should be lower than the elastic prediction which does not account for damage. Furthermore, the greater the extent of damage the greater the predicted discrepancy between G_1 and A_1. This is precisely what is seen in Figure 10.

Evaluation of the Total Resistance Moment

The total resistance moment R_t was taken to be the volume of transformed material associated with a crack advance normalized with respect to the crack surface created as a result of that crack advance. In other words, it was computed as

$$R_t = dV/t_0\, dl$$

where dV is the volume change of the active zone associated with crack advance dl and t_0 is the original sample thickness. The results of this calculation are plotted as a function of crack length in Figure 11.

Evaluation of the Energy Dissipation Rate

The rate of energy dissipation on damage creation within the active zone is given by

$$\dot{D} = \dot{W}_i - \dot{Q}$$

where $\dot{W}_i$ is the rate of work done on irreversible deformation and $\dot{Q}$ is the rate of heat dissipation during this process. Since the rate of heat dissipation could not be measured $\dot{D}$ was expressed as

$$\dot{D} = \beta \dot{W}_i$$

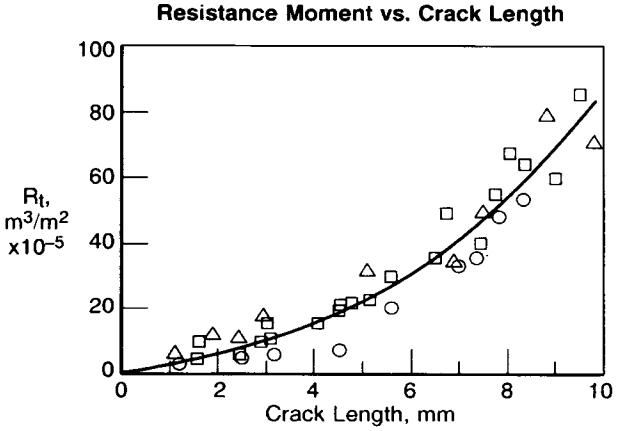

Fig. 11. Total resistance moment plotted as a function of crack length for three HDPE fatigue specimens. Mean stress is 7.94 MPa.

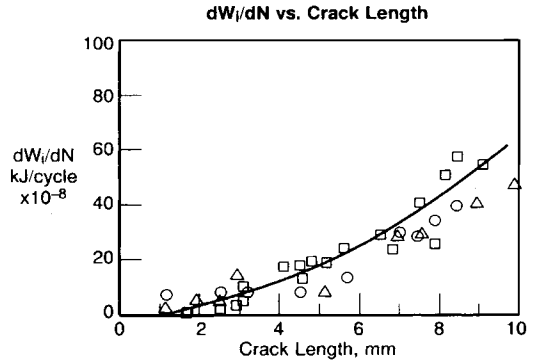

Fig. 12. Rate of irreversible work plotted as a function of crack length for three HDPE fatigue specimens. Mean stress is 7.94 MPa.

where β is a coefficient that reflects the portion of $\dot{W}_i$ expended on damage formation. It can be thought of as a measure of efficiency for the process of damage creation.

Experimentally $\dot{W}_i$ at a given crack length is measured as the difference in area between the hysteresis loop obtained at the crack length in question and that obtained prior to initiation. The results are shown in Figure 12. These results in conjunction with resistance moment data from Figure 11 can be readily understood within our paradigm of concurrent damage mechanisms.

In the "brittle" regime a relatively small amount of material is transformed, thus requiring a low rate of energy dissipation. As the yielding mechanism becomes more prominent in the "ductile" regime ($l > 4.5$ mm), a progressively larger amount of material is transformed, resulting in a rapidly increasing rate of energy dissipation.

Evaluation of β and γ*

In accordance with the model of concurrent damage mechanisms, it is not unreasonable to suggest that each of them may very well possess a different specific enthalpy (γ^*) and characteristic energy dissipation coefficient (β). As such, the "brittle" and "ductile" kinetic regimes should be analyzed separately.

The law of CL propagation can be rewritten as

$$A_1/R_t = -\beta \dot{W}_i/(t_0 R_t\, dl/dt) + \gamma^*$$

Thus, a plot of A_1/R_t vs. $\dot{W}_i/(t_0 R_t\, dl/dt)$ should produce a straight line with slope $-\beta$ and intercept γ^*. Such plots for the two kinetic regions are shown in Figures 13 and 14 along with the calculated β and γ^* values. Crack speed values calculated from the law of CL propagation are compared with observed values in Table I. The agreement is very encouraging.

An important observation must immediately be made. Specific enthalpy values for the dominant mechanisms of damage in the "brittle" and "ductile" regions are indistinguishable within the level of accuracy afforded by the experimental procedure. This is not entirely surprising, for if the values were

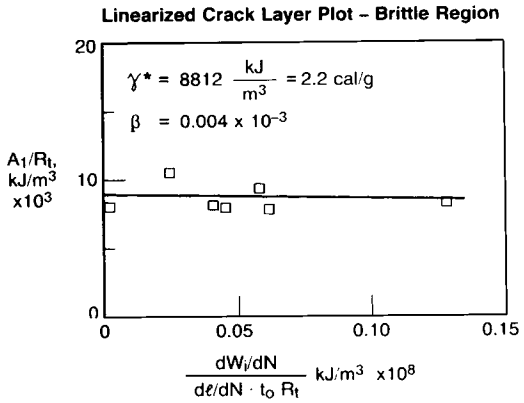

Fig. 13. Linearized crack layer plot for the "brittle" region of HDPE fatigue. Mean stress is 7.94 MPa.

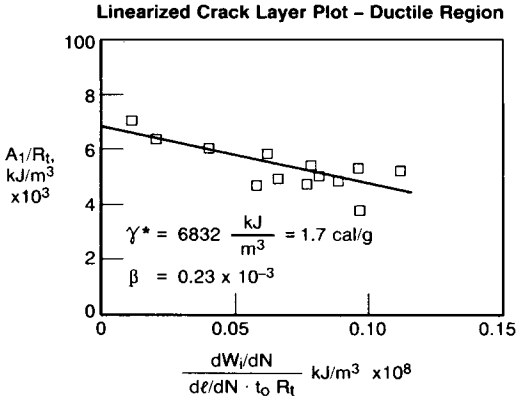

Fig. 14. Linearized crack layer plot for the "ductile" region of HDPE fatigue. Mean stress is 7.94 MPa.

TABLE I
Comparison of Observed HDPE Fatigue Crack Propagation Rates with Crack Layer Results

	Crack layer fit	
l (mm)	Observed dl/dN (m/cycle $\times 10^{-8}$)	Calculated dl/dN (m/cycle $\times 10^{-8}$)
1.25	2.45	2.44
2.56	3.40	0.91
2.95	1.46	0.34
3.10	1.36	0.32
4.60	11.0	11.0
4.80	12.0	16.7
5.65	13.0	12.9
6.55	20.0	12.3
7.45	23.0	31.0
8.05	26.0	29.5
8.80	26.7	31.3

dramatically different, it is doubtful that the two damage mechanisms would appear concurrently.

Effect of Stress Level on HDPE Fatigue Behavior

The crack layer analysis undertaken above would be of little value if the mechanism of HDPE fatigue fracture were a strong function of the stress level. To investigate this issue, fatigue fracture of HDPE under a mean stress of 3.75 MPa and otherwise identical experimental conditions were observed and analyzed. The results are compared with those obtained earlier under 7.94 MPa in Figures 15–19. Obviously, HDPE fracture behavior under 3.75 MPa is qualitatively identical to that observed at 7.94 MPa. Although there are the expected quantitative differences in crack speed, energy release rate, resistance moment, and energy dissipation rate, the functional similarity of the plots is undeniable. It should be noted that the onset of accelerated fracture surface "thinning" in Figure 16 occurs at a much longer crack length for the 3.75 MPa stress level. This suggests a far more extensive "brittle" regime at the lower stress, which is, of course, quite intuitive.

While the functional similarity of relevant fracture parameters is convincing, the most powerful argument in favor of mechanistic similarity of HDPE fatigue failure at different stress levels is contained in Figure 20. Here the total resistance moment R_t is plotted as a function of energy release rate for

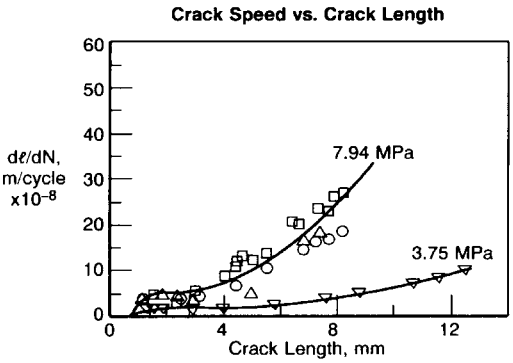

Fig. 15. Crack speed plotted vs. crack length for 3.75 and 7.94 MPa HDPE fatigue samples.

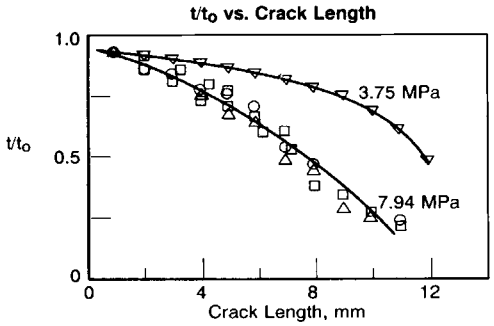

Fig. 16. Thinning profiles for 3.75 MPa and 7.94 MPa fatigue samples.

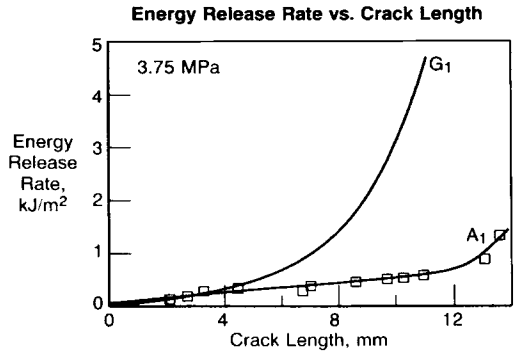

Fig. 17. Total potential energy release rate plotted as a function of crack length. Elastic energy release rate shown also. Mean stress is 3.75 MPa.

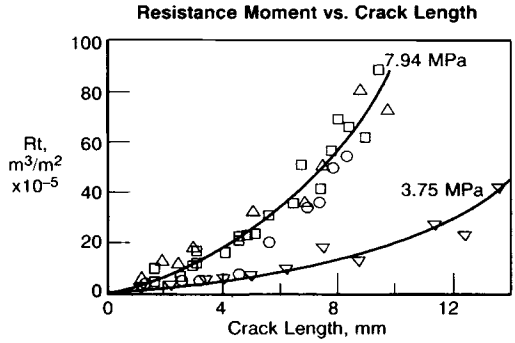

Fig. 18. Total resistance moment plotted vs. crack length for 3.75 and 7.94 MPa fatigue.

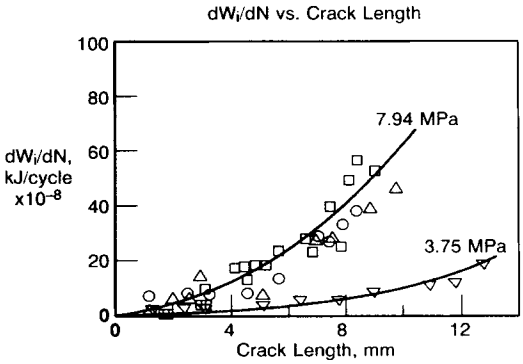

Fig. 19. Rate of irreversible work plotted vs. crack length for 3.75 and 7.94 MPa fatigue.

the two different stress levels. If the mechanism of failure is unchanged, then the amount of transformed material at a given energy release rate should be independent of stress level. This is precisely what is seen in Figure 20.

A direct consequence of the mechanistic similarity argument is the implied constancy of the specific enthalpy of damage at the two different stress levels. Figures 21 and 22 contain the linearized CL plots for the 3.75 MPa data.

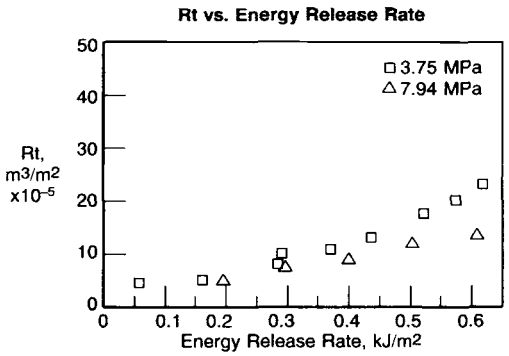

Fig. 20. Total resistance moment plotted vs. energy release rate for 3.75 and 7.94 MPa fatigue.

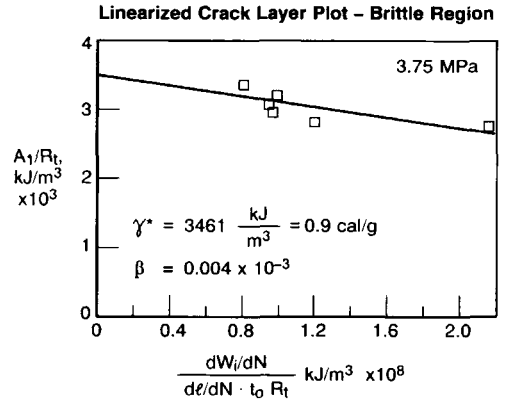

Fig. 21. Linearized crack layer plot for the "brittle" region of 3.75 MPa HDPE fatigue.

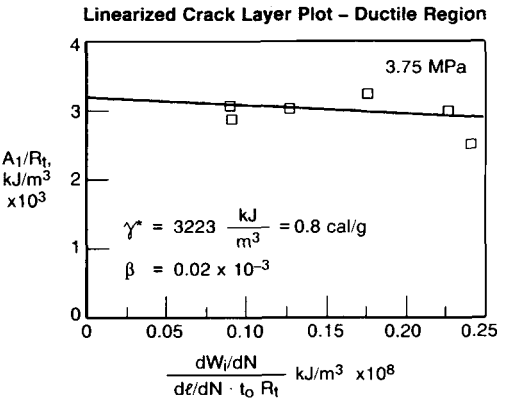

Fig. 22. Linearized crack layer plot for the "ductile" region of 3.75 MPa HDPE fatigue.

Calculated "brittle" and "ductile" γ^* values are once again indistinguishable within experimental error, but they are inspiringly close to those obtained for the 7.94 MPa samples. Furthermore, an earlier study in this laboratory conducted at a 5.63 MPa stress level produced γ^* values of 1.3 and 0.9 cal/g for the brittle and ductile regimes, respectively [Ref. 15, corrected for several calculational errors].

CONCLUSIONS

1. Fatigue crack propagation in HDPE occurs with an accompanying layer of damage.
2. Fatigue crack propagation behavior of HDPE exhibits three kinetic regions. Of these, initiation and "deceleration" (constant crack speed) regions are extremely reproducible, while the crack acceleration region is subject to significant sample to sample variation.
3. Ultimate failure occurs through uncontrolled yielding of the unbroken ligament.
4. Two damage mechanisms responsible for HDPE fatigue failure have been identified:
   (i) fibrillated void formation;
   (ii) yielding.
   Both mechanisms are present throughout the entire range of crack propagation, though voiding is dominant in the "brittle" regime, while yielding is much more preponderant in the "ductile" regime.
5. HDPE fatigue fracture has been observed to be mechanistically identical at two different stress levels.
6. The crack layer theory has been applied successfully to HDPE fatigue crack propagation. The analysis produced values of γ^*, the specific enthalpy of damage, in the 1–2 cal/g range.

References

1. M. K. V. Chan and J. G. Williams, *Int. J. Fracture*, **23**, 145 (1983).
2. A. Lustiger, R. L. Markham, and M. M. Epstein, *J. Appl. Polym. Sci.*, **26**, 1049 (1981).
3. C. S. Lee and M. M. Epstein, *Polym. Eng. Sci.*, **22**, 9 (1982).
4. G. P. Marshall, L. E. Culver, and J. G. Williams, *Plast. Polym.* (Apr.), 95–101 (1970).
5. J. G. Williams and G. P. Marshall, *Proc. Roy. Soc. London*, **A342**, 55 (1975).
6. S. Bandhyopadhyay and H. R. Brown, *Polymer*, **22**, 245 (1981).
7. P. C. Paris, M. P. Gomez, and W. E. Anderson, *Found. Eng.*, **13**, 9 (1961).
8. C. B. Bucknall and P. Dumpleton, *Polym. Eng. Sci.*, **256**, 313, (1985).
9. A. Chudnovsky, *Tenth U.S. Nat. Cong. Appl. Mech.*, August 1986, p. 97.
10. A. Chudnovsky and A. Moet, *J. Mater. Sci.*, **20**, 630 (1985).
11. E. H. Andrews and B. J. Walker, *Proc. Roy. Soc. London*, **A325**, 57 (1971).
12. S. Bandyopadhyay and H. R. Brown, *Int. J. Fracture*, **15**, R175 (1979).
13. P. E. Bretz, R. W. Hertzberg, and J. A. Manson, *Polymer*, **22**, 575 (1981).
14. K. Tonyali and H. R. Brown, *J. Mater. Sci.*, **21**, (1986).
15. K. Sehanobish, A. Moet, and A. Chudnovsky, *Polymer*, **28**, 1315 (1987).
16. A. S. Saada, *Elasticity: Theory and Applications*, Krieger, Florida, 1983.
17. A. Chudnovsky, unpublished.
18. N. Haddaoui, Ph.D. thesis, Case Western Reserve Univ., 1986.
19. J. A. Begley and J. D. Landes, *ASTM STP514*, ASTM, Philadelphia, 1972, pp. 1–39.
20. M. Ben Ouezdou, Ph.D. thesis, Case Western Reserve Univ., 1987.

Received September 19, 1988
Accepted December 16, 1988